Effect of Drag Reducers on Transport Phenomena in Turbulent Pipe Flow

Peter J. Hamersma and Jan M. H. Fortuin
University of Amsterdam, Dept. of Chemical Engineering, 1018 WV Amsterdam, The Netherlands

Momentum transfer in turbulent pipe flows ($d = 51$ mm) with and without a drag reducer was studied. Age distributions of coherent fluid structures at the pipe wall were determined at different Reynolds numbers ($10^4 < Re < 6 \times 10^4$) using laser-Doppler velocimetry (LDV) and a suitable discriminating procedure. Mean ages, mean transfer thicknesses, friction factors, and time-averaged axial velocity profiles derived from LDV signals were compared with those from axial pressure gradients using the random surface-renewal model. The distribution of the ages was random, and drag reducers increased the mean age and the mean transfer thickness of the fluid elements at the wall, thus decreasing momentum and heat transfer at the fluid–wall interface. The mechanism of single-surface renewals was derived from conditionally averaged, local axial fluid velocities obtained from LDV signals.

Introduction

In chemical engineering, there is still a need for a reliable model to calculate transfer coefficients at the interface in turbulent fluid flows with a drag reducer in such a way that the chemical engineer can use it with understanding and confidence in many applications.

Research on phenomena occurring in the wall region of turbulent pipe flows and the effect of drag reducers on the flow behavior are relevant for:

- Improving the physical understanding of heat, mass, and momentum transfer in turbulent fluid flows.
- Designing efficient heat exchangers to save energy and to reduce investment costs in plants.
- Investigating fouling that not only reduces the capacity of heat exchangers, but also the production capacity and safety of a plant.
- Optimizing the conditions for fluid transport in pipelines, for example, to decrease the pressure gradient and the heat-transfer coefficient in pipelines; more particularly in low-temperature areas.
- Improving conditions for polyolefin production in long tube reactors, where a high molecular fraction of the product can act as a drag and heat-transfer reducer in a supercritical fluid flow.

In a previous article, momentum transfer in turbulent pipe flows was described using the random surface-renewal (RSR) model in which drag reducers were assumed to increase the mean age of fluid elements at the wall (Fortuin and Klijn, 1982), leading to friction reduction. With laser-Doppler velocimetry (LDV), it has subsequently been shown that for turbulent *Newtonian* fluid flows in a pipe, the age distribution of fluid elements at the wall is random and that the mean age is dependent on the tube diameter, and the velocity and viscosity of the fluid (Van Maanen and Fortuin, 1983; Musschenga et al., 1992). The age distribution and mean ages of fluid elements at the wall of turbulent Newtonian fluid flows in pipes determined with LDV at different Reynolds numbers have been used to predict heat, mass, and momentum transfer at the interface and to derive the Chilton–Colburn analogy (Fortuin et al., 1992). In the present article, investigations with LDV are presented concerning the effect of a low concentration of a *drag reducer* in turbulent pipe flow on the age distribution and mean age of fluid elements, and on momentum and heat transfer at the wall. Friction factors derived from LDV measurements will be compared with those obtained from axial pressure gradients.

The scope of the present article on turbulent pipe flow with and without a drag reducer is:

- To study the behavior of coherent fluid structures during a surface renewal.
- To investigate the effect of a drag reducer on both surface renewal and momentum transfer at the wall.

Correspondence concerning this article should be addressed to J. M. H. Fortuin.
Current address of P. J. Hamersma: Delft University of Technology, Faculty of Applied Sciences, Julianalaan 136, 2628 BL Delft, The Netherlands.

- To derive the *age distribution*, *mean age*, and *mean transfer thickness* of fluid elements at the wall from both LDV signals and axial pressure gradients.
- To determine whether the values of the mean age, mean transfer thickness, friction factor, and time-averaged axial velocity profiles in the wall region, derived from LDV signals, agree with those obtained from axial pressure gradients using the RSR model.
- To model the mechanism of surface renewals and to verify the model with conditionally averaged local axial fluid velocities obtained from LDV signals.

RSR Model

Momentum transfer

In describing momentum transfer from a turbulent fluid flow to the tube wall, the curvature of the wall is neglected and the axial velocity in the bulk is assumed to be approximately equal to the superficial velocity. These approximations are only valid if the ratio of the mean momentum-transfer thickness and the tube radius is very small ($\bar{\delta}/R < 0.05$). This condition approximately holds at $Re > 10^4$. In turbulent pipe flows, fluid elements from the bulk can replace fluid elements at the wall. Upon its arrival at the wall, an inrushing fluid element gradually loses momentum by viscous interaction with the wall. In this fluid element, which originally traveled with a uniform bulk velocity, u_b, a velocity profile starts to develop when the interface is reached. Then the development of this velocity profile, and the unsteady momentum transfer from the laminar fluid element to the wall, can be described by the following reduced equation of motion and appropriate initial and boundary conditions

$$\frac{\partial u(y,t)}{\partial t} = \nu \frac{\partial^2 u(y,t)}{\partial y^2};\ I.C.:\ t = 0\ \ y > 0\ \ u(y,t) = u_b \quad (1)$$

$$B.C.:\ t > 0\ \ y = 0\ \ u(y,t) = 0;$$

$$B.C.:\ t > 0\ \ y = \infty\ \ u(y,t) = u_b.$$

Integration of Eq. 1 results in the following relative instantaneous, axial velocity profile in a fluid element at the wall

$$\frac{u(y,t)}{u_b} = \mathrm{erf}(z)$$

where

$$\mathrm{erf}(z) = \frac{2}{\sqrt{\pi}} \int_0^z e^{-z^2} dz \quad \text{and} \quad z = \frac{y}{2\sqrt{\nu t}}. \quad (2)$$

As a result of LDV measurements (Van Maanen and Fortuin, 1983), it has been shown that, in the time domain, laminar Newtonian fluid elements at an arbitrary position at the wall are randomly renewed by fluid elements from the turbulent core and that the average period, t_0, between successive renewals affects the pressure gradient. Using these considerations and Eq. 2, the local time-averaged axial velocity profile in the wall region, which is representative for each position at the wall, follows from

$$\frac{\bar{u}(y)}{u_b} = \int_0^\infty \{\mathrm{erf}(z)\}\{\exp(-t/t_0)\}\, d(t/t_0). \quad (3)$$

Partial integration of Eq. 3 results in the relative time-averaged axial velocity profile in the laminar fluid elements at the wall

$$\frac{\bar{u}(y)}{u_b} = 1 - \frac{2}{\sqrt{\pi}} \int_0^\infty \exp\left[-\left(z^2 + z_0^2/z^2\right)\right] dz =$$

$$1 - \exp(-2z_0);\ z_0 = \frac{y}{2\sqrt{\nu t_0}}. \quad (4)$$

The time-averaged local axial shear stress at the wall, $\bar{\tau}_w$, exerted by randomly renewed laminar fluid elements can be derived from Eq. 4

$$\bar{\tau}_w = \eta \left[\frac{\partial \bar{u}(y)}{\partial y}\right]_{y=0} = \frac{\nu \rho u_b}{\sqrt{\nu t_0}}. \quad (5)$$

At $Re > 10^4$, it can be assumed that $u_b \approx \langle \bar{u} \rangle$. Then, Eq. 5 and the definition of the Fanning friction factor

$$f \equiv \frac{\bar{\tau}_w}{\frac{1}{2}\rho \langle \bar{u} \rangle^2}, \quad (6)$$

where $\bar{\tau}_w = \Delta p d/(4L)$, results in the friction factor of a Newtonian fluid flow (Fortuin and Klijn, 1982)

$$f = 2\left[\frac{d}{\sqrt{\nu t_0}}\right]\left[\frac{\nu}{\langle \bar{u} \rangle d}\right] = 2Fo^{-1/2}Re^{-1};$$

$$Fo^{-1/2} = Ref/2 \equiv Fa;\quad \bar{\delta} = \sqrt{\nu t_0};\quad Re > 10^4, \quad (7)$$

where $\bar{\delta}$ is the mean momentum-transfer thickness. For dilute drag-reducer solutions, the friction factor f_p and the drag-reduction factor f_{dr} follow from

$$f_p \equiv \bar{\tau}_{w,p} \Big/ \left(\frac{1}{2}\rho \langle \bar{u} \rangle^2\right);\quad \bar{\tau}_{w,p} = \Delta p_p d/(4L);$$

$$f_{dr} \equiv f_p/f. \quad (8)$$

Assuming that the high-shear viscosity at the wall is approximately equal to that of the solvent, the friction factor f_p of the turbulent flow of a dilute polymer solution, with randomly distributed ages of fluid elements at the wall, follows from

$$f_p = 2\left[\frac{d}{\sqrt{\nu t_{0,p}}}\right]\left[\frac{\nu}{\langle \bar{u} \rangle d}\right] = 2Fo_p^{-1/2}Re^{-1};$$

$$\bar{\delta}_p = \sqrt{\nu t_{0,p}};\quad Re > 10^4, \quad (9)$$

where $t_{0,p}$ is the mean age and $\bar{\delta}_p$ is the mean momentum-transfer thickness of the dilute polymer solution.

As a result, Eqs. 7–9 lead to

$$f_{dr} \equiv f_p/f = \left(t_0/t_{0,p}\right)^{1/2} = \bar{\delta}/\bar{\delta}_p. \quad (10)$$

Using Eqs. 4 and 7, the mean axial velocity profile in the wall region of a turbulent pipe flow without and with a drag reducer, respectively, follows from

$$\frac{\bar{u}(y)}{\langle \bar{u} \rangle} = 1 - \exp\left(-y/\sqrt{\nu t_0}\right); \quad \frac{\bar{u}_p(y)}{\langle \bar{u} \rangle} = 1 - \exp\left(-y/\sqrt{\nu t_{0,p}}\right) = 1 - \exp\left(-f_{dr} Fa \frac{y}{d}\right). \quad (11)$$

Heat transfer

In turbulent pipe flow, heat transfer can also be described with the RSR model (Fortuin et al., 1992). The following equations can be derived from this model:

$$Nu = C\left(\frac{f}{2}\right) RePr^{1/3}; \quad \text{(Newtonian fluid flow)} \quad (12)$$

$$Nu_p = C\left(\frac{f_p}{2}\right) RePr^{1/3}; \quad \text{(Polymer-solution flow)}, \quad (13)$$

where

$$C = \frac{(\pi/6)^{1/3}}{\Gamma(4/3)} = 0.9026; \quad Re > 10^4; \quad Pr > 1. \quad (14)$$

Equations 10, 12, and 13 lead to

$$Nu_p/Nu = \alpha_p/\alpha = f_{hr} = f_p/f = f_{dr} = \sqrt{t_0/t_{0,p}}. \quad (15)$$

Equation 15 shows that for turbulent pipe flows of dilute drag-reducer solutions and a sufficiently high wall shear stress ($Re > 10^4$), the heat-transfer reduction factor, f_{hr}, is approximately equal to the drag-reduction factor, f_{dr}. Deviations from Eq. 15 can be caused by fouling of the wall, by thermal and mechanical degradation of the polymer, and/or by radial viscosity gradients in the wall region. Addition of a drag reducer to a turbulent pipe flow reduces not only the friction factor, but also the heat-transfer coefficient. This is particularly important for applications in pipelines in low-temperature areas.

Experimental Studies

Figure 1 shows a view of the setup, consisting of the test section, LDV, and data-processing equipment. The transfer of momentum, heat, and mass from the core of a turbulent pipe flow to the wall is governed by the diameter of the tube, the velocity and viscosity of the fluid and, according to the RSR model, also by the ages of the fluid elements at the tube wall. The age distribution and the mean age of these fluid

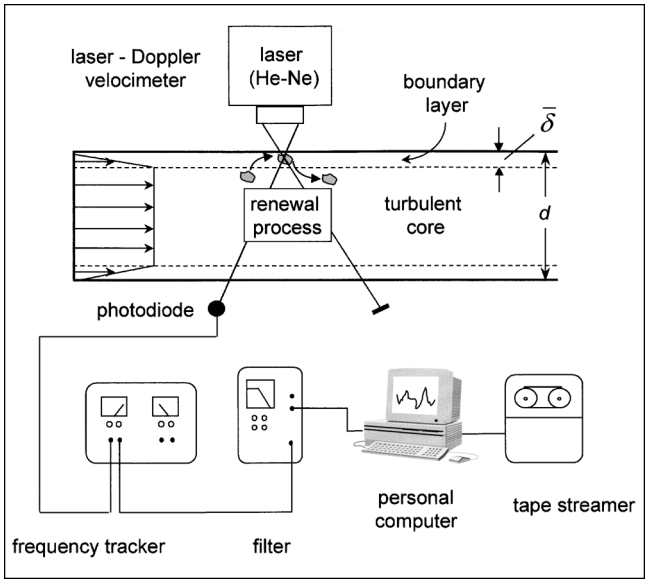

Figure 1. Test section with laser-Doppler velocimeter and data-processing equipment.

elements can be derived from velocity signals recorded in the time domain with the LDV during steady-state turbulent pipe flow, followed by a suitable discrimination procedure to detect the surface renewals. The variable age, t, is the period between two successive detected renewals at the same position at the wall. The time-averaged value of these periods is t_0. The mean swap time, t_s, can be obtained from the distance between the abscissa of the average minimum and maximum axial velocity in two exchanging fluid elements, measured with LDV at a small distance from the wall. It will be shown that in the range $10^4 < Re < 6 \times 10^4$, the mean swap time, t_s, is an order of magnitude smaller than t_0 and approximately proportional to t_0 (see the Appendix).

Pipe and fluids

The setup consists of a 51-mm-ID, smooth copper pipe with a total length of 30 m. This pipe has a horizontal, straight measuring section of 8.5 m, containing a 1.4-m precision glass tube ($d = 51.0$ mm). This tube is situated 5.5 m beyond the entrance of the measuring section, so that there is sufficient entry and exit length for the turbulent fluid flow to be fully developed in the glass tube.

At a small distance, y, from the wall of the glass tube (Figure 1), the velocity of light-scattering particles in the beams-intersection volume (the "eye") of two coherent laser beams of a LDV is used to measure the instantaneous local axial fluid velocity [$u(y,t)$]. Tap water has been used for the investigations of the single-phase pipe flow. The liquid flow rate is controlled with valves and rotameters covering superficial velocities $\langle \bar{u} \rangle$ in the glass tube between 0.034 $m \cdot s^{-1}$ and 3.4 $m \cdot s^{-1}$. The actual mass flow rate is determined by weighing the amount of water leaving the pipe in a measured time interval at a constant mass flow rate. Application of this method results in a value of the mass flow rate with an error less than 0.2%. A water manometer has been applied to mea-

sure the pressure drop over a pipe length of 5.89 m. The error in the pressure drop ranges from 0.5 Pa to 5 Pa, depending on the angle of inclination of the manometer. Light-scattering particles, necessary for LDV measurements, have been supplied from a vessel containing diluted milk using a rotary displacement pump. The diluted milk is injected through an injection port placed 9.75 m upstream of the glass tube. The concentration of the milk in the turbulent flow is approximately 50 mg/kg.

A concentrated polymer solution (2,000 mg/kg Separan AP-30 in water) is injected into the turbulent water flow 12 m before the test section using a pressure vessel. The polymer concentration in the turbulent water flow can be adjusted using a control valve and a rotameter.

The master batch is prepared by solving 300-g Separan AP-30 (a polyacrylamide with a relative molecular mass of about $3 \cdot 10^6$) in 150 kg demineralized water and adding an aqueous sodiumhydroxide solution until the solution has a pH of 10 in order to stabilize the viscous properties of the polymer solution. This solution is gently stirred for 12 h to obtain a homogeneous solution without degradation of the polymer that is ready for injection into the turbulent water flow. Values of the three viscosity parameters that characterize the non-Newtonian laminar flow behavior of aqueous solutions of Separan AP-30 covering concentrations ranging from 0 to 5,000 mg/kg, and shear stresses from 10^{-4} Pa to 300 Pa, have been reported in a previous article (Hamersma et al., 1983). The three concentration-dependent viscosity parameters refer to apparent viscosities at shear rates zero and infinite and to a yield stress. For an aqueous solution of 20 mg/kg Separan AP-30, the values of three concentration-dependent parameters at 20°C are $\eta_0 = 5.4$ mPa·s, $\eta_\infty = 1.15$ mPa·s, and $\tau_0 = 0.03$ Pa.

The laser-Doppler velocimeter

An LDV, operating in the reference-beam mode, was used. This arrangement was chosen for its ease of alignment and the good signal-to-noise ratio (SNR) in cases where many light-scattering particles transverse the beams-intersection volume, called the eye. The LDV consists of a Spectra Physics 15 mW He–Ne laser (wave length 632.8 nm) and quality optics, assembled by the Institute of Applied Physics TNO-TU Delft, The Netherlands. In the optical arrangement used, the angle between the two laser beams was 20.96°, which resulted in an eye (beams-intersecting volume), with a length of $b = 214\ \mu$m at a beam diameter of $b_0 = 39\ \mu$m in air, where $b = b_0/\sin(10.48°)$. The LDV is mounted on an optical bench, which enables precise movement of the measuring volume in two directions perpendicular to the axis of the tube. The signals were processed in a similar way, as was described in a previous article (Fortuin et al., 1992).

Detection criterion

At a small distance, y, from the wall, local instantaneous axial velocities were measured in the time domain using LDV. Renewals were detected using a modified version of the Blackwelder and Kaplan (BK) detection criterion (1976). The BK detection criterion reacts on the fluctuations of the difference $u' = u(y,t) - \bar{u}(y)$ of the instantaneous local axial velocity $u(y,t)$ and the time-averaged local axial velocity $\bar{u}(y)$, at a distance y from the wall. The BK criterion detects both sharp local accelerations and sharp local decelerations of fluid elements in axial direction. In the modified version, *accelerations* ($\partial u'/\partial t > 0$) will only be considered as renewals, while the decelerations ($\partial u'/\partial t < 0$) will not be taken into account.

Using the modified BK criterion, a surface renewal is assumed to occur if

$$\frac{\left(\overline{(u')^2}^{\,a}\right) - \left(\overline{(u')}^{\,a}\right)^2}{\left(\overline{(u')^2}^{\,\mathrm{ent}}\right)} \geq k \quad \text{and} \quad \frac{\partial u'}{\partial t} > 0,$$

where

$$u' = u(y,t) - \bar{u}(y). \tag{16}$$

In Eq. 16, $\overline{\ }^{a}$ denotes a time averaging over a short period, a, that is of the order of the mean swap time t_s; $\overline{\ }^{\mathrm{ent}}$ means a time averaging over the *entire* signal during a sufficiently long period; and k is a dimensionless threshold value. The values of the averaging period, a, and the threshold value, k, should be chosen in such a way that sharp accelerations are detected and white noise is ignored. Fully objective values of a and k cannot be found in an independent way, because no independent calibration data are available. The number of surface renewals we have to find under any given set of experimental conditions is unknown. The detection criterion can only give well-defined, objective values of the ages, t, if a and k have objective values.

Detection parameters a and k

In studying the instantaneous local axial velocities measured in the time domain, we observed that with increasing values of Re, both the mean swap time, t_s, and the mean age, t_0, decrease. The averaging period a needed for the detection of a renewal can be considered as the width of a window in the time domain. The value of a should be sufficiently large to detect a renewal and to ignore white noise. However, a should not be larger than the mean renewal interval, so that some renewals could not be detected. Therefore, it is useful to attribute a value to a of the order of the mean swap time, t_s.

In a limited range of Reynolds numbers, the mean swap time, t_s, may be assumed to be proportional to the mean age, t_0. This assumption and Eqs. 7 and 9 lead to the conclusion that the averaging periods, a and a_p, may be chosen in such a way that for a turbulent pipe flow

- without a drag reducer:

$$a = \gamma t_0; \quad t_0 = (d/Fa)^2/\nu; \quad Fa \equiv Ref/2 \tag{17}$$

- with a drag reducer:

$$a_p = \gamma t_{0,p}; \quad t_{0,p} = \{d/(f_{dr} Fa)\}^2/\nu, \tag{18}$$

where γ is a constant.

The axial pressure gradients measured in the isothermal, steady-state turbulent water flows in the glass tube used could

be well described by the following friction-factor correlation from the literature (Eck, 1978)

$$f = 0.07725\{\log(Re/7)\}^{-2} \text{ and}$$

$$Fa = 0.03863\,Re\{\log(Re/7)\}^{-2}; \quad 2{,}300 < Re < 10^8. \quad (19)$$

Using Eqs. 17 and 18, it has been shown (Fortuin et al., 1992) that for LDV measurements on Newtonian liquids at Reynolds numbers between 10^4 and $45 \cdot 10^3$, the following dimensionless detection parameters $\gamma = a/t_0 = a_p/t_{0,p} = 0.0348$ and $k = 1.13$ may be applied. As a consequence, the averaging time a and the threshold value k become:

$$a = 0.0348 t_0; \; a_p = 0.0348 t_{0,p}; \; k = 1.13;$$

$$10^4 < Re < 45 \times 10^3 \text{ or } 39 < Fa < 120, \quad (20)$$

in which t_0 and $t_{0,p}$ can be obtained from Eqs. 17 to 19.

The threshold level $k = 1.13$ has been fixed in such a way that, at $Re = 15 \times 10^3$, the friction factor, f_{LDV}, calculated with Eq. 7, using the mean age $(t_0)_{\text{LDV}}$ derived from LDV signals, is equal to the friction factor, f, obtained from Eq. 19, based on pressure-drop measurements. Assuming γ and k are independent of the Reynolds number, the mean ages, $(t_0)_{\text{LDV}}$, at other Reynolds numbers of the turbulent water flow can be derived from the measured velocity signals using Eqs. 16 and 17 and the same values of the detection parameters, γ and k, as have been applied at $Re = 15 \times 10^3$ (Musschenga et al., 1992). For drag-reducer solutions, a similar procedure has been used to calculate $(t_{0,p})_{\text{LDV}}$ obtained from LDV signals using Eqs. 16 and 18 and equal values of the dimensionless detection parameters $\gamma = 0.0348$ and $k = 1.13$.

Constraints

The applied method has its limitations. If $Re < (Re)_{\min}$, with for example, $(Re)_{\min} = 5{,}000$, the relatively large momentum-transfer thickness, $\bar{\delta}$, may not be neglected with regard to the radius of the tube. Then, the approximation $u_b \approx \langle \bar{u} \rangle$ is not valid and the internal curvature of the pipe should also be taken into account. If $Re > (Re)_{\max}$, with for example, $(Re)_{\max} = 45{,}000$, the laser-beam diameter and the length of the eye are not negligibly small with respect to the momentum-transfer thickness. Therefore, it can be expected that only LDV measurements in the limited range $(Re)_{\min} < Re < (Re)_{\max}$ will lead to acceptable experimental results. The set-point $f_{\text{LDV}} = f$ was chosen at $Re = \{(Re)_{\min}(Re)_{\max}\}^{0.5} = 15{,}000$. Further, it can be expected that, at $(Re)_{\max} > 45{,}000$, the undetected renewals can only be observed with a larger SNR. This would be possible if a laser beam with a smaller diameter, more sensitive detection equipment, and less noise could be applied. In addition, it has to be taken into account that the values $\gamma = 0.0348$ and $k = 1.13$ can only be considered as constants in a restricted range of Reynolds numbers.

Results

Newtonian fluid flows

Table 1 shows results derived from local, instantaneous axial velocities measured with LDV in the wall region of isothermal, steady-state, turbulent water flows at thirteen different Reynolds numbers (column one). In columns two and three, the temperatures and the kinematic viscosities of the solvent flows are given. Each line of column four shows the number N_0 of the detected ages at the related Reynolds number. In column five, the mean ages, t_0, calculated with Eqs. 17 and 19 are presented. Column six shows the values of $(t_0)_{\text{LDV}}$, derived from LDV signals using Eqs. 16 and 17 with $a = 0.0348\ t_0$ and $k = 1.13$. For the thirteen different Reynolds numbers, the same values of the dimensionless detection parameters, $\gamma = 0.0348$ and $k = 1.13$, were applied. The values of γ and k were chosen in such a way that at $Re = 15{,}000$, $f_{\text{LDV}}/f = 1$, where f_{LDV} follows from Eq. 7 and $t_o = (t_0)_{\text{LDV}}$, and f from Eq. 19, based on pressure-gradient measurements (column seven). Age distributions and mean ages of fluid elements at the pipe wall derived from axial velocity measurements obtained from LDV signals have already been presented for Newtonian fluid (NF) flows as histograms at *five* different Reynolds numbers in two previous articles (Fortuin et al., 1992; Musschenga et al., 1992). These histograms, derived from LDV signals, show that in turbulent water flows in straight, smooth tubes, the number N of detected ages between t and $t + \Delta t$ can be represented by (Van Maanen and Fortuin, 1983)

$$N/\Delta t = (N_0/t_0)\exp(-t/t_0), \quad (21)$$

where N, N_0, t, and the mean age, $t_o = (t_0)_{\text{LDV}}$, follow from LDV measurements and the detection procedure of Eq. 16, with $a = 0.0348 t_0$ and $k = 1.13$.

It has been seen that, in turbulent NF flows at these five Reynolds numbers ($10^4 < Re < 45 \times 10^3$), the ages of fluid elements at the wall are randomly distributed and that equal mean ages are obtained from LDV signals and pressure gradients. These phenomena show that the chance of detecting a surface renewal in an isothermal turbulent NF flow at an arbitrary position at the pipe wall is constant in the time domain, at fixed values of d, ν, and $\langle \bar{u} \rangle$, and independent of the age of the fluid element at the wall.

Table 1. NF Flows: Physical Quantities Referring to LDV Measurements in Turbulent Water Flows through a Horizontal Straight and Smooth Tube*

1 $Re/10^3$	2 T/K	3 $10^6\nu/(\text{m}^2 \cdot \text{s}^{-1})$	4 $N_0/1$	5 t_0/s	6 $(t_0)_{\text{LDV}}/\text{s}$	7 f_{LDV}/f
12.1	289.3	1.10	3350	1.189	1.163	1.011
15.0	281.3	1.38	5435	0.690	0.690	1.000
19.5	289.4	1.10	5439	0.587	0.592	0.996
24.3	288.8	1.12	9182	0.414	0.412	1.003
31.3	291.7	1.04	5759	0.304	0.293	1.018
37.2	292.8	1.02	4252	0.267	0.238	1.059
40.2	290.3	1.08	5863	0.199	0.190	1.025
42.7	292.8	1.01	6158	0.194	0.185	1.025
43.4	293.1	1.00	5595	0.191	0.184	1.020
49.9	292.8	1.01	2141	0.153	0.198	0.878
55.5	288.4	1.13	1767	0.116	0.457	0.503
57.3	291.9	1.03	1145	0.121	0.272	0.667
59.0	292.8	1.01	2430	0.118	0.280	0.649

*$y^+ = 36$; $d = 0.051$ m; $\gamma = 0.0348$; $k = 1.13$; set point $Re = 15 \times 10^3$.

Table 2. PS Flows; Physical Quantities Referring to LDV Measurements in Turbulent Aqueous Polymer-Solution Flows (20 mg/kg Separan AP-30) Through a Horizontal Straight and Smooth Tube

1 $Re/10^3$	2 $10^6\nu/(m^2\cdot s^{-1})$	3 $N_{0,p}/1$	4 $f_{dr}/1$	5 $t_{0,p}/s$	6 $(t_{0,p})_{LDV}/s$	7 $(f_p)_{LDV}/f_p$
12.1	1.10	3237	0.965	1.280	1.250	1.011
19.1	1.10	8591	0.873	0.794	0.690	1.073
24.5	1.12	10024	0.860	0.553	0.526	1.026
27.8	1.02	7171	0.841	0.524	0.474	1.052
31.1	1.05	6784	0.790	0.487	0.472	1.016
37.2	1.02	5158	0.759	0.413	0.365	1.064
40.3	1.07	4735	0.686	0.426	0.365	1.081
42.5	1.00	2647	0.680	0.428	0.369	1.077
43.8	1.00	5775	0.716	0.368	0.318	1.076
47.0	1.04	5302	0.726	0.309	0.310	0.998
49.9	1.05	4783	0.692	0.307	0.326	0.970
55.8	1.13	883	0.600	0.319	1.020	0.559
59.8	1.02	1874	0.647	0.273	0.599	0.675

Note: $y_p^+ = 36$; $d = 0.051$ m; $\gamma = 0.0348$; $k = 1.13$; setpoint $Re = 15\times10^3$ at $f_{dr} = 1$.

Polymer-solution flows

Table 2 shows results obtained with aqueous polymer-solution (PS) flows. The drag reduction factors, f_{dr}, of column four have been derived from axial pressure-gradient measurements. Figure 2a and 2b show the age distributions of fluid elements at the wall of turbulent PS flows (20 mg/kg Separan AP-30 in water) at $Re = 12{,}100$ and $Re = 31{,}100$, repectively. The histograms were derived from LDV signals. The number N_p of detected ages between t and $t + \Delta t$ has been respresented by the solid curves obtained from

$$N_p/\Delta t = \left(N_{0,p}/t_{0,p}\right)\exp\left(-t_p/t_{0,p}\right), \qquad (22)$$

in which N_p, $N_{0,p}$, t_p, and $t_{0,p} = (t_{0,p})_{LDV}$ follow from LDV measurements (Table 2) using the detection procedure of Eq. 16 with $a = 0.0348t_{0,p}$ and $k = 1.13$. Figure 2a and 2b show that in turbulent PS flows, the ages of fluid elements at the pipe wall are also randomly distributed. Summarizing, it can be stated that random surface renewals, which were hypothetical events proposed by Danckwerts (1951) to describe mass transfer at an interface of turbulent fluid flows, now appear to be *existing phenomena* in turbulent pipe flows with and without a drag reducer that can be observed at different Reynolds numbers with LDV.

Mean ages

In Figure 3, the dimensionless mean ages Fo and Fo_p were plotted against Re. The dashed line refers to NF flows and has been calculated with $Fo = Fa^{-2}$ and Eq. 19. The open circles refer to $Fo_{LDV} = \nu(t_0)_{LDV}/d^2$ using $(t_0)_{LDV}$ from Table 1. The solid circles indicate values of $(Fo_p)_{LDV} = \nu(t_{0,p})_{LDV}/d^2$ using $(t_{0,p})_{LDV}$ from Table 2. The solid triangles were calculated from $Fo_p = (f_{dr}Fa)^{-2}$ using f_{dr} from Table 2 and Fa from Eq. 19. A best-fit procedure to all solid markers yields the solid line representing the correlation

$$Fo_p = 6.26Re^{-1.00} \text{ or } t_{0,p} = 6.26d/\langle\bar{u}\rangle; \quad 10^4 < Re < 5\times10^4. \qquad (23)$$

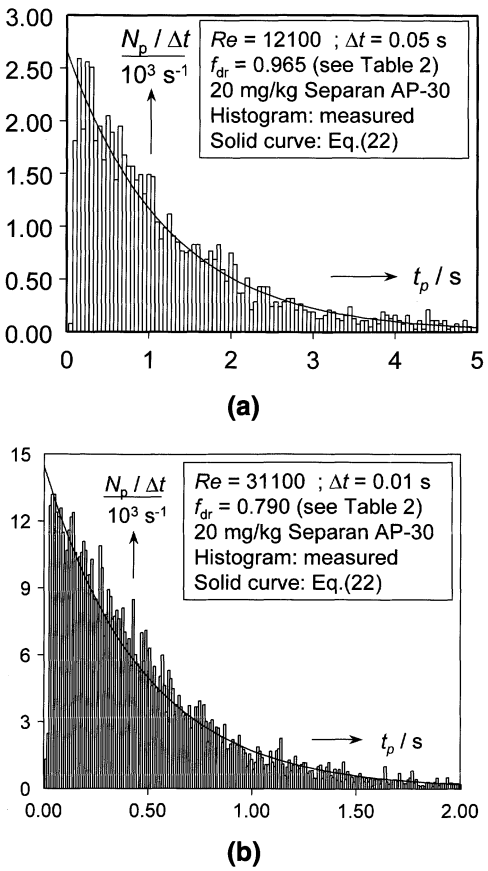

Figure 2. Age distributions of fluid elements at the wall in turbulent pipe flows of an aqueous drag-reducer solution at (a) $Re = 12{,}100$, and (b) $Re = 31{,}100$.

Histograms represent the age distributions from LDV signals, using Eq. 16 with $a_p = 0.0348\ t_{0,p}$ and $k = 1.13$. The value of $t_{0,p}$ was calculated with Eqs. 18 and 19 after using f_{dr} from pressure-drop measurements and Eq. 8.

Figure 3 shows that at equal values of Reynolds:

$$Fo_p = f_{dr}^{-2}Fo > Fo \text{ and}$$

$$(Fo_p)_{LDV} = Fo_{LDV}(t_{0,p})_{LDV}/(t_0)_{LDV} > Fo_{LDV}. \qquad (24)$$

This means that small concentrations of a drag reducer increase the mean age of fluid elements at the wall in the region $10^4 < Re < 5\times10^4$.

Mean momentum-transfer thickness

For a turbulent NF flow in a straight smooth tube, the dimensionless mean momentum transfer thickness can be obtained from Eqs. 7 and 19

$$\bar{\delta}/R = \sqrt{\nu t_0}\,/R = 2Fa^{-1} = 51.8Re^{-1}\{\log(Re/7)\}^2;$$

$$10^4 < Re < 45\times10^3. \qquad (25)$$

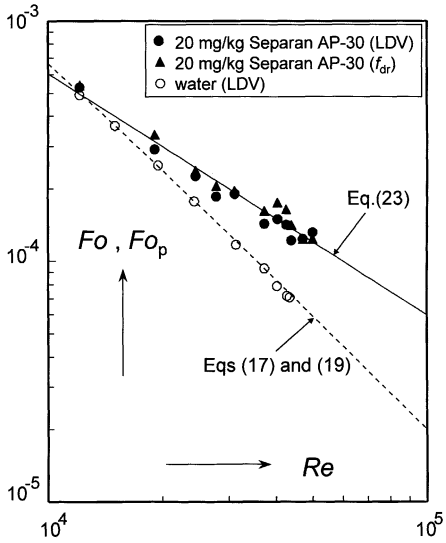

Figure 3. Dimensionless mean ages $Fo = \nu t_0/d^2$ and $Fo_p \equiv \nu t_{0,p}/d^2$ of fluid elements at the wall of turbulent pipe flows of water and an aqueous drag-reducer solution (20 mg/kg Separan AP-30) as a function of the solvent Reynolds number *Re*.

Open circles were obtained from Table 1 and solid markers from Table 2.

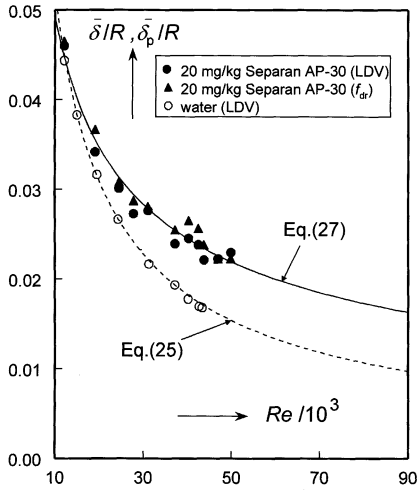

Figure 4. Relative mean transfer thicknesses $\bar{\delta}/R$ and $\bar{\delta}_p/R$ in turbulent pipe flows of water and an aqueous drag-reducer solution (20 mg/kg Separan AP-30) as a function of the solvent Reynolds number *Re*.

Open circles were obtained from Table 1 and solid markers from Table 2.

The dashed curve in Figure 4 obtained with Eq. 25 gives the relationship between the mean momentum transfer thickness of a turbulent water flow and the Reynolds number. The open circles in this figure refer to values of $\bar{\delta}_{\mathrm{LDV}}/R$ derived from ν values in column three of Table 1 and the mean ages presented in column six of Table 1. For a drag-reducer solution flow in a straight smooth tube Eqs. 9, 10, and 25 yield

$$\bar{\delta}_p/R = \sqrt{\nu t_{0,p}}\,/R = 2(f_{dr}Fa)^{-1}$$

$$= 51.8(f_{dr}Re)^{-1}\{\log(Re/7)\}^2; \qquad 10^4 < Re < 5\times 10^4. \quad (26)$$

The solid circles in Figure 4 refer to $(\bar{\delta}_p)_{\mathrm{LDV}}/R$ calculated with $(t_{0,p})_{\mathrm{LDV}}$ presented in column six of Table 2. The solid triangles in this figure were obtained with Eq. 26 after substitution of the drag-reduction factor, f_{dr}, presented in Table 2 and derived from pressure-gradient measurements.

A best-fit procedure applied to the solid markers yields the solid line in Figure 4 and the following correlation

$$\bar{\delta}_p/R = 5.0Re^{-0.502}; \quad 10^4 < Re < 5\times 10^4. \quad (27)$$

The results presented in Figure 4 show that

$$\bar{\delta}_p/R = f_{dr}^{-1}(\bar{\delta}/R) > (\bar{\delta}/R); \quad 10^4 < Re < 45\times 10^3$$

$$(\bar{\delta}_p)_{\mathrm{LDV}}/R = \{(t_{0,p})_{\mathrm{LDV}}/(t_0)_{\mathrm{LDV}}\}^{1/2}(\bar{\delta}_{\mathrm{LDV}}/R)$$

$$> (\bar{\delta}_{\mathrm{LDV}}/R). \quad (28)$$

This means that a small concentration of a drag reducer in a turbulent fluid flow increases the mean momentum-transfer thickness. The difference $\Delta\bar{\delta}/R$ can be obtained from Eqs. 25 and 26

$$\Delta\bar{\delta}/R = (\bar{\delta}_p - \bar{\delta})/R = 2Fa^{-1}(f_{dr}^{-1} - 1). \quad (29)$$

The solid triangles in Figure 5 were obtained from Eqs. 29 and the values of f_{dr} from Table 2. The solid line in this figure was derived from Eqs. 25 and 27, and can be represented by the correlation

$$\Delta\bar{\delta}/R = (\bar{\delta}_p - \bar{\delta})/R = 5.0Re^{-0.502} - 51.8Re^{-1}\{\log(Re/7)\}^2. \quad (30)$$

Figure 5 shows that at increasing values of *Re*, the value of $\Delta\bar{\delta}$ approaches a limit value. As a result, the decrease of f_{dr}, and consequently the effect of the drag reducer, is limited too.

Friction factors

In Figure 6, two ratios of friction factors have been plotted against *Re*. These ratios derived from Eqs. 7 to 10 can be represented by

$$\frac{f_{\mathrm{LDV}}}{f} = \frac{d}{Fa\sqrt{\nu(t_0)_{\mathrm{LDV}}}} = \sqrt{\frac{t_0}{(t_0)_{\mathrm{LDV}}}};$$

$$\frac{(f_p)_{\mathrm{LDV}}}{f_p} = \frac{d}{f_{dr}Fa\sqrt{\nu(t_{0,p})_{\mathrm{LDV}}}}$$

$$= \sqrt{\frac{t_{0,p}}{(t_{0,p})_{\mathrm{LDV}}}}, \quad (31)$$

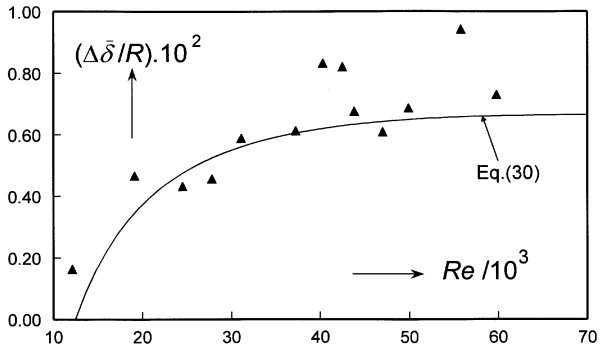

Figure 5. Relative difference $\Delta\bar{\delta}/R$ between mean transfer thicknesses of the flow of the aqueous drag-reducer solution (20 mg/kg Separan AP-30) and that of water as a function of the solvent Reynolds number.

Solid triangles were obtained from Eqs. 29 and 19 using f_{dr} from Table 2.

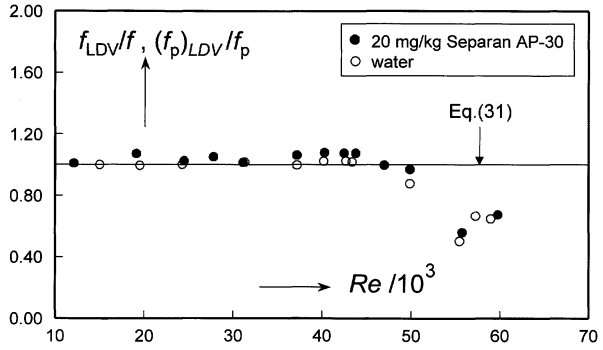

Figure 6. Ratios f_{LDV}/f of a turbulent water flow (Table 1) and $(f_p)_{LDV}/f_p$ of a turbulent flow of an aqueous drag-reducer solution (Table 2) plotted against the solvent Reynolds number.

where the Fanning number (Fa) can be derived from Eq. 19. Results obtained with water flows and PS flows were presented in Tables 1 and 2, respectively. Figure 6 shows that for turbulent liquid flows with and without a drag reducer, in the region $10^4 < Re < 5\times10^4$, the values of the friction factors, derived from LDV signals using the RSR model, agree with those obtained from pressure-drop measurements. Further, it appears that at $Re > 5\times10^4$, friction factors derived from LDV signals are too small. These deviations, which already were discussed in the subsection titled "Constraints," are a result of the limitations of the equipment used and the procedure applied. At values of $Re > 5\times10^4$, some renewals cannot be detected in the time domain, because the related accelerations are too short to be distinguished from noise. In that case, the remaining LDV signals yield values of $(t_0)_{LDV}$ and $(t_{0,p})_{LDV}$ that are too large, resulting in values of f_{LDV} and $(f_p)_{LDV}$ that are too small.

Axial velocity profiles in the wall region

Measured and simulated time-averaged axial velocity profiles in isothermal turbulent pipe flows are presented in Figure 7. The irregular solid line in this figure shows the time-averaged axial velocity profile of an *aqueous solution* of 20 mg/kg Separan AP-30 measured in the wall region, with an LDV, at $Re = 26\times10^3$ ($T = 282$ K, $\nu = 1.36\times10^{-6}$ m$^2\cdot$s^{-1}). This velocity profile agrees with the simulated dotted velocity profile calculated with Eqs. 11 and 19. This figure further shows that, at increasing values of y, the two velocity profiles approach $u_b \approx \langle\bar{u}\rangle$ asymptotically. The smooth solid curve, which represents the simulated velocity profile of a water flow ($f_{dr} = 1$) for similar conditions, has also been calculated with Eqs. 11 and 19. From Figure 7 it can be concluded that good agreement exists between measured and simulated velocity profiles of a PS flow, and that in the wall region at a fixed distance from the wall a drag reducer decreases the time-averaged axial velocity. At a constant superficial velocity this decrease is compensated by a small increase of the fluid velocity in the bulk that can be neglected at higher Reynolds numbers ($Re > 10^4$).

Mechanism of a surface renewal

In this section, a study of the behavior of fluid elements at the wall in turbulent pipe flows with and without a drag reducer are reported. At a surface renewal, an inrushing fluid element from the bulk with a velocity u_b is assumed to penetrate between the old fluid element and the wall, while the old one is swapped to the bulk. These events can be derived from axial velocities measured with LDV in the eye at a small distance, y, from the wall. During the surface renewal the old fluid element and the new one successively pass the eye in the wall-to-bulk direction, while the instantaneous, local, axial velocity in the eye is recorded using LDV.

Measured velocities

Instantaneous axial velocities were measured in the time domain at a small distance, y, from the wall, and surface re-

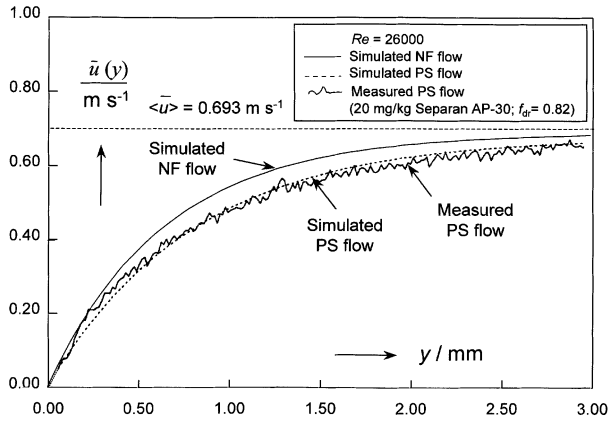

Figure 7. Time-averaged axial velocity profiles in the wall region of turbulent pipe flows at Re = 26,000 ($T = 282$ K; $\nu = 1.36\times10^{-6}$ m$^2\cdot$s^{-1}).

Irregular solid line was derived from LDV signals and refers to a turbulent flow of the aqueous drag-reducer solution. Dotted curve and smooth solid line were simulated using Eqs. 11 and 19, after substituting $f_{dr} = 0.82$ for the PS flow and $f_{dr} = 1$ for the NF flow.

newals were detected in the usual way. Velocities measured at time, t, around a detection time, t_d, were recorded. Velocities measured at equal $t - t_d$ values were averaged and presented as a *conditionally averaged local axial* (CALA) velocity at a distance, y, from the wall. In Figure 8, CALA velocities, $\hat{u}$, derived from LDV signals of turbulent pipe flows with and without a drag reducer, were plotted against the difference $(t - t_d)$ between the variable time, t, and the detection time, t_d, of the surface renewal. The dotted curves refer to CALA velocities in turbulent NF flows; the solid curves to turbulent PS flows. Because each curve has been obtained by averaging a large number of detected renewals, the random-velocity fluctuations have been averaged out so that the CALA velocities around the detection time remain.

Figure 8 shows that the observed velocity rise $((d\hat{u}/dt)$ at the detection time $t = t_d$ increases with increasing values of the Reynolds number and that the CALA velocity around the detection time suddenly rises from a minimum value $\hat{u}_{\min} \approx \langle \bar{u} \rangle/2$ to a maximum value $\hat{u}_{\max}$, which approaches the superficial velocity $\langle u \rangle$ in the pipe. Only at the lowest Reynolds number, $(Re = 12{,}100)$, does $(\hat{u})_{\max}$ exceed $\langle \bar{u} \rangle$. This phenomenon is due to the fact that the assumption $u_b \approx \langle u \rangle$, made after Eq. 5, does not hold at low Reynolds numbers, because the low volume-flow rate through the *thicker* boundary layer must be compensated by a *higher* velocity $u_b > \langle \bar{u} \rangle$ in the bulk to obtain the superficial velocity, $\langle \bar{u} \rangle$, in the tube. Comparing the CALA velocities of turbulent flows with and without a drag reducer, it has to be taken into account that the CALA velocities obtained with and without a drag reducer have been measured at equal y^+ values $(y^+ = 36 = y_p^+)$, and as a result at different y values $(y_{36} \neq y_{p,36}$; Table 3).

Simulated TALA velocities

The universal velocity profile in the wall region of a turbulent pipe flow is usually presented by the following dimensionless distances from the wall (Fortuin and Klijn, 1982):

$$y^+ \equiv (y/\nu)(\bar{\tau}_w/\rho)^{0.5} \quad \text{(NF flow)};$$

$$y_p^+ \equiv (y_p/\nu)(\bar{\tau}_{w,p}/\rho)^{0.5} \quad \text{(PS flow)}. \quad (32)$$

Equations 6, 8 and 32 yield the following distances between the eye (beams-intersection volume) and the wall

$$y = y^+ d\, Re^{-1}\sqrt{2/f} \quad \text{(NF flow)}; \quad y_p = y_p^+ d\, Re^{-1}\sqrt{2/f_p} \quad \text{(PS flow)} \quad (33)$$

$$y_{36} = 36 d\, Re^{-1}\sqrt{2/f} \quad \text{(NF flow)}; \quad y_{p,36} = 36 d\, Re^{-1}\sqrt{2/f_p} \quad \text{(PS flow)}, \quad (33a)$$

where $y_{36} = y$ at $y_{36}^+ = 36$ and $y_{p,36} = y_p$ at $y_{p,36}^+ = 36$.

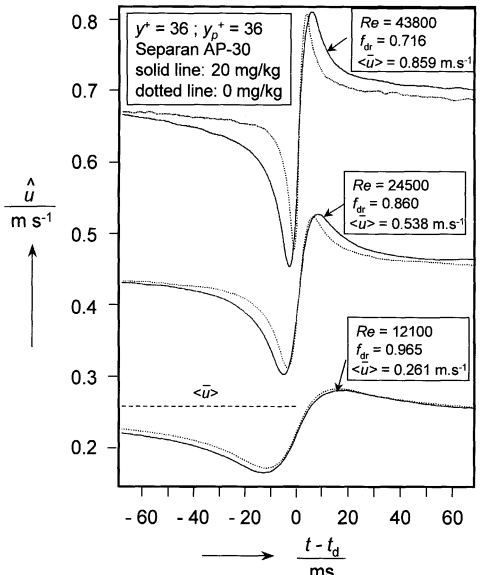

Figure 8. Measured CALA velocities at $y_p^+ = 36$ (solid lines) and at $y^+ = 36$ (dotted lines) plotted against the difference between the time, t, and the detection time, t_d.

Curves refer to isothermal turbulent pipe flows, three with and three without a drag reducer at solvent Reynolds numbers in Table 3.

Table 3. Physical Quantities Referring to Six Turbulent Pipe Flows

	Three NF Flows				Three PS Flows			Eq.
$Re \cdot 10^{-3}$	12.1	24.3	43.4	$Re \cdot 10^{-3}$	12.1	24.5	43.8	7
Fa	44.6	74.9	116.6	Fa	44.6	75.4	117.4	19
f_{dr}	1.000	1.000	1.000	f_{dr}	0.965	0.860	0.716	10
$f \cdot 10^3$	7.37	6.16	5.37	$f_p \cdot 10^3$	7.11	5.29	3.84	8, 19
ϵ	2.185	1.998	1.866	ϵ_p	2.147	1.851	1.577	36
y_{36}/mm	2.500	1.361	0.816	$y_{p,36}$/mm	2.545	1.457	0.957	33
$\langle \bar{u} \rangle/(\mathrm{m \cdot s^{-1}})$	0.261	0.534	0.851	$\langle \bar{u} \rangle/\mathrm{m \cdot s^{-1}}$	0.261	0.538	0.859	—
$[\bar{u}(y_{36})]/(\mathrm{m \cdot s^{-1}})$	0.232	0.462	0.719	$[\bar{u}(y_{p,36})]/(\mathrm{m \cdot s^{-1}})$	0.231	0.453	0.682	38
$(\nu \cdot 10^6)/(\mathrm{m^2 \cdot s^{-1}})$	1.10	1.12	1.00	$(\nu \cdot 10^6)/(\mathrm{m^2 \cdot s^{-1}})$	1.10	1.12	1.00	—
$\hat{u}_{\min}/(\mathrm{m \cdot s^{-1}})$	0.173	0.313	0.479	$\hat{u}_{p,\min}/(\mathrm{m \cdot s^{-1}})$	0.164	0.303	0.453	Fig. 8
$\hat{u}_{\max}(\mathrm{m \cdot s^{-1}})$	0.285	0.525	0.810	$\hat{u}_{p,\max}/(\mathrm{m \cdot s^{-1}})$	0.284	0.528	0.811	Fig. 8
$(t_{\min} - t_d)$/ms	−11.2	−3.1	−0.7	$(t_{p,\min} - t_d)$/ms	−12.3	−4.5	−2.5	Fig. 8
$(t_{\max} - t_d)$/ms	14.4	6.6	4.3	$(t_{p,\max} - t_d)$/ms	16.1	8.6	6.3	Fig. 8
$\Delta_{\min}$/ms	−12.8	−4.9	−2.5	$\Delta_{p,\min}$/ms	−14.2	−6.5	−4.4	41
$\Delta_{\max}$/ms	12.8	4.9	2.5	$\Delta_{p,\max}$/ms	14.2	6.5	4.4	42
Δ_0/ms	12.8	4.9	2.5	$\Delta_{0,p}$/ms	14.2	6.5	4.4	42
$\bar{\delta}$/mm	1.14	0.681	0.438	$\bar{\delta}_p$/mm	1.19	0.79	0.61	25, 26
$u_{wb}/(\mathrm{m \cdot s^{-1}})$	0.112	0.174	0.220	$u_{wb,p}/\mathrm{m \cdot s^{-1}}$	0.102	0.152	0.174	A14
t_0/s	1.19	0.414	0.191	$t_{0,p}$/s	1.28	0.553	0.368	17, 18
t_s/t_0	0.0215	0.0237	0.0262	$t_{s,p}/t_{0,p}$	0.0228	0.0235	0.0239	40
$t_d - t_r$/ms	1.6	1.7	1.8	$(t_d - t_{r,p})$/ms	2.4	2.1	1.9	41

Further, Eqs. 7 and 9 lead to

$$\sqrt{\nu t_0} = d\,Re^{-1}(2/f) \quad \text{(NF flow)};$$

$$\sqrt{\nu t_{0,p}} = d\,Re^{-1}(2/f_p) \quad \text{(PS flow)}. \tag{34}$$

Equations 33 and 34 yield the dimensionless distances

$$y/\sqrt{\nu t_0} = y^+/\sqrt{2/f} \quad \text{(NF flow)};$$

$$y_p/\sqrt{\nu t_{0,p}} = y_p^+/\sqrt{2/f_p} \quad \text{(PS flow)}. \tag{35}$$

The CALA velocities were measured with LDV at $y^+ = 36$ (NF flow) and $y_p^+ = 36$ (PS flow). For these conditions, the dimensionless distances between eye and wall are

$$\epsilon = \frac{y_{36}}{\sqrt{\nu t_0}} = \frac{36}{\sqrt{2/f}} \quad \text{(NF flow)};$$

$$\epsilon_p = \frac{y_{p,36}}{\sqrt{\nu t_{0,p}}} = \frac{36\sqrt{f_{dr}}}{\sqrt{2/f}} \quad \text{(PS flow)}, \tag{36}$$

where, according to Eq. 19,

$$\sqrt{2/f} = 5.088 \log(Re/7). \tag{37}$$

Equations 11, 35, and 36 lead to the time-averaged local axial (TALA) velocities in the eye

$$\bar{u}(y_{36}) = \langle \bar{u} \rangle \{1 - \exp(-\epsilon)\} \quad \text{(NF flow)};$$

$$\bar{u}_p(y_{p,36}) = \langle \bar{u} \rangle \{1 - \exp(-\epsilon_p)\} \quad \text{(PS flow)}. \tag{38}$$

Table 3 shows values of physical quantities concerning isothermal turbulent pipe flows, three without and three with a drag reducer, based on measurements at different Reynolds numbers. Additionally, information concerning these flows is given in Table 1 and Table 2 at equal Reynolds numbers. Further, Figure 8 shows that each measured profile of the CALA velocities consists of three regions, bounded by a minimum and a maximum CALA velocity.

Simulated CALA velocities

A model for CALA velocities is derived in the Appendix, and presented in Table 4 for both NF flows and PS flows. CALA velocities can be simulated with the following equations

$$\hat{u}(y) = \langle \bar{u} \rangle \left[1 - \exp\left\{ -\epsilon \left[1 + \left(\frac{\Delta}{\Delta_0} \right) \exp\left(-\frac{1}{2} \frac{\Delta^2}{\Delta_0^2} \right) \right] \right\} \right];$$

$$\hat{u}_p(y_p) = \langle \bar{u} \rangle \left[1 - \exp\left\{ -\epsilon_p \left[1 + \left(\frac{\Delta_p}{\Delta_{0,p}} \right) \exp\left(-\frac{1}{2} \frac{\Delta_p^2}{\Delta_{0,p}^2} \right) \right] \right\} \right]. \tag{39}$$

If $y^+ \neq 36$ and/or $y_p^+ \neq 36$, the values of ϵ and ϵ_p have to be replaced by Fay/d and $f_{dr}Fay/d$, respectively.

Equations for the minimum values at $\Delta/\Delta_0 = -1$ or $\Delta_p/\Delta_{0,p} = -1$, and the maximum values at $\Delta/\Delta_0 = 1$ or $\Delta_p/\Delta_{0,p} = 1$ are presented in Table 4. The distance between the horizontal coordinates of the minimum and maximum CALA velocity is defined as the mean swap time, t_s. Therefore, Eq. 39 leads to

$$t_s \equiv 2\Delta_0 \equiv t_{\max} - t_{\min}$$

Table 4. Equations for Simulating TALA and CALA Velocities

TALA Velocity NF Flow (at $y^+ = 36$) $\bar{u}(y_{p,36}) = \langle \bar{u} \rangle \{1 - \exp(-\epsilon)\}$ $\epsilon = \dfrac{y_{36}}{\sqrt{\nu t_0}} = \dfrac{36}{\sqrt{2/f}} = \dfrac{7.08}{\log(Re/7)}$	TALA Velocity PS Flow (at $y_p^+ = 36$) $\bar{u}_p(y_{p,36}) = \langle \bar{u} \rangle \{1 - \exp(-\epsilon_p)\}$ $\epsilon_p = \dfrac{y_{p,36}}{\sqrt{\nu t_{o,p}}} = \dfrac{36\sqrt{f_{dr}}}{\sqrt{2/f}} = \dfrac{7.08\sqrt{f_{dr}}}{\log(Re/7)}$
CALA Velocities NF Flow (at $y^+ = 36$) $\hat{u}(y_{36}) = \langle \bar{u} \rangle \left[1 - \exp\left\{ -\epsilon \left[1 + \left(\dfrac{\Delta}{\Delta_0} \right) \exp\left(-\dfrac{1}{2} \dfrac{\Delta^2}{\Delta_0^2} \right) \right] \right\} \right]$ At $\dfrac{\Delta}{\Delta_0} = -1$; $\{\hat{u}(y_{36})\}_{\min} = \langle \bar{u} \rangle \left[-\exp\left\{ -\epsilon \left[-\exp\left(1 - \dfrac{1}{2} \right) \right] \right\} \right]$ At $\dfrac{\Delta}{\Delta_0} = 0$; $\{\hat{u}(y_{36})\}_{\Delta=0} = \langle \bar{u} \rangle [1 - \exp(-\epsilon)]$ At $\dfrac{\Delta}{\Delta_0} = 1$; $\{\hat{u}(y_{36})\}_{\max} = \langle \hat{u} \rangle \left[1 - \exp\left\{ -\epsilon \left[1 + \exp\left(-\dfrac{1}{2} \right) \right] \right\} \right]$	CALA Velocities PS Flow (at $y_p^+ = 36$) $\hat{u}_p(y_{p,36}) = \langle \bar{u} \rangle \left[1 - \exp\left\{ -\epsilon_p \left[1 + \left(\dfrac{\Delta_p}{\Delta_{0,p}} \right) \exp\left(-\dfrac{1}{2} \dfrac{\Delta_p^2}{\Delta_{0,p}^2} \right) \right] \right\} \right]$ At $\dfrac{\Delta_p}{\Delta_{0,p}} = -1$; $\{\hat{u}_p)(y_{p,36})\}_{\min} = \langle \bar{u} \rangle \left[1 - \exp\left\{ -\epsilon_p \left[1 - \exp\left(-\dfrac{1}{2} \right) \right] \right\} \right]$ At $\dfrac{\Delta_p}{\Delta_{0,p}} = 0$; $\{\hat{u}_p(y_{p,36})\}_{\Delta=0} = \langle \bar{u} \rangle [1 - \exp(-\epsilon_p)]$ At $\dfrac{\Delta_p}{\Delta_{0,p}} = 1$; $\{\hat{u}_p(y_{p,36})\}_{\max} = \langle \bar{u} \rangle \left[1 - \exp\left\{ -\epsilon_p \left[1 + \exp\left(-\dfrac{1}{2} \right) \right] \right\} \right]$

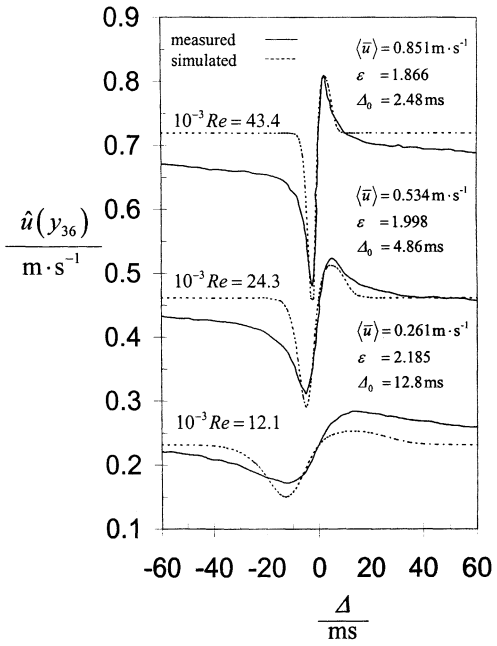

Figure 9. Measured and simulated CALA velocities at $y^+ = 36$ plotted against the difference Δ between the time, t, and the reference time, t_r, in turbulent pipe flows of water at Reynolds numbers in Table 3.

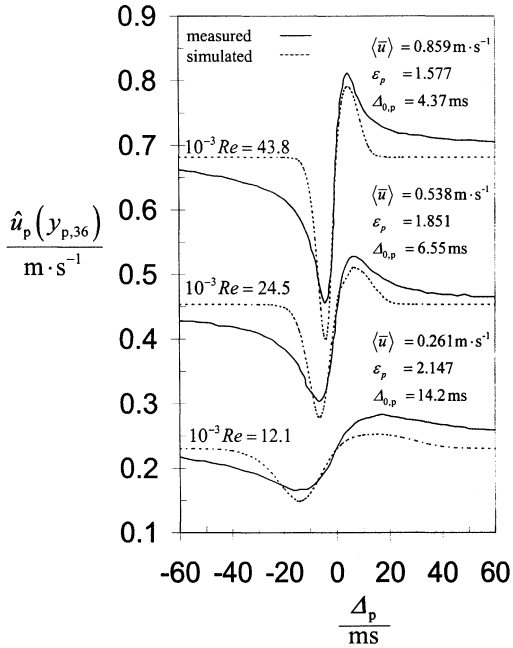

Figure 10. Measured and simulated CALA velocities at $y_p^+ = 36$ plotted against the difference Δ_p between the time t and the reference time t_r in turbulent pipe flows of aqueous, 20 mg/kg Separan AP-30 solutions at solvent Reynolds numbers presented in Table 3.

for NF flow, and

$$t_{s,p} \equiv 2\Delta_{0,p} \equiv t_{p,\max} - t_{p,\min} \tag{40}$$

for PS flow.

It has to be noted that t_s is an order of magnitude smaller than t_0 and that t_s is approximately proportional to t_0, so that t_s/t_0 is approximately constant, as was shown in the second last line of Table 3. Figure 9 shows measured and simulated CALA velocities of water flows, and Figure 10 of aqueous PS flows (20 mg/kg Separan AP-30). The simulated results were obtained using the data of Table 3 and the equations of Table 4.

Comparison of measured and simulated velocities

For a comparison of measured and simulated results, the subjective detection time t_d of Figure 8 has to be replaced by an objective reference time, t_r, based on two measured values, $t_{\min}$ and $t_{\max}$, related to the minimum and maximum CALA velocity. As a result of this consideration, the following physical quantities were introduced

$$t_r \equiv (t_{\min} + t_{\max})/2; \qquad \Delta \equiv t - t_r;$$

$$|\Delta_0| \equiv |t_{\min} - t_r| = t_{\max} - t_r; \qquad t_r - t_d = (t_{\max} - t_d) - \Delta_{\max} \tag{41}$$

$$\Delta_{\min} \equiv t_{\min} - t_r; \qquad \Delta_{\max} \equiv t_{\max} - t_r; \qquad \Delta p \equiv t_p - t_{r,p}$$

$$\Delta_{p,\min} \equiv t_{p,\min} - t_{r,p}; \qquad \Delta_{p,\max} \equiv t_{p,\max} - t_{r,p}. \tag{42}$$

The ratio t_s/t_0 of the distance t_s between the horizontal coordinates of the extreme $\hat{u}$ values of each profile in Figure 8, and t_0 is also presented in Table 3. This ratio appears to be approximately constant, as was assumed in the section titled "Detection Parameters a and k." The solid curves in Figures 9 and 10 refer to the same measured CALA velocities as were presented in Figure 8. However, the $(t - t_d)$ axis was replaced by the Δ or Δp axis, using Eqs. 41 and 42.

The dotted lines of Figures 9 and 10 refer to simulated CALA velocities at equal conditions. They were obtained using the parameter values of Table 3 and the equations of Table 4.

Comparison of the profiles shows a reasonable agreement between the measured and simulated results. The differences between these results can be ascribed to imperfections in the model and errors in the parameters used. A discussion about these items is added to the derivation of the model in the Appendix.

Conclusions

- Laser-Doppler velocity (LDV) measurements have validated the random surface renewal (RSR) model for transport phenomena in turbulent pipe flows with and without a drag reducer.

• Addition of a drag reducer to a turbulent pipe flow, at constant values of ν, d, and $\langle \bar{u} \rangle$, increases the mean age and mean momentum transfer thickness of fluid elements at the wall, resulting in a decrease in both the friction factor and the heat-transfer coefficient.

• The heat-transfer reduction factor is approximately equal to the drag-reduction factor at equal solvent Reynolds numbers ($Re > 10^4$), low drag-reducer concentrations, and small radial viscosity gradients.

• In steady-state turbulent pipe flows of liquids without ($10 \times 10^3 < Re < 43 \times 10^3$) and with ($10 \times 10^3 < Re < 50 \times 10^3$) a drag reducer, it has been shown that:

—The age distribution of fluid elements at the wall is always random;

—The friction factors (f_{LDV}) and ($f_p)_{\mathrm{LDV}}$), derived from LDV signals, are equal to the friction factors (f and f_p) obtained from pressure-drop measurements;

—the time-averaged axial velocity profile of a turbulent pipe flow in the wall region, derived from the friction factor with the RSR model, agrees with the average profile obtained from LDV signals.

• The RSR model not only describes the transfer of momentum and heat in turbulent pipe flows, but also the mechanism and the CALA velocities of surface renewals. Therefore, the chemical engineer can apply it with understanding and confidence to describe momentum and heat transfer in the wall region of fully developed steady-state turbulent fluid flows with and without a drag reducer in straight, smooth tubes.

Acknowledgments

The authors thank the Netherlands Foundation for Chemical Research (SON) for financial aid from the Netherlands Organization for Scientific Research (NWO) and Messrs. E.E. Musschenga, J. Ellenberger, E. Grolman, C.S. Bildea, and J. Zoutberg and his coworkers for their contribution in the Universiteit van Amsterdam to this study.

Notation

a = averaging period in Eq. 17, s
a_p = averaging period in Eq. 18, s
b_0 = diameter of laser beams, m
b = length of eye (beams-intersection volume), m
C_p = heat capacity of fluid, $\mathrm{J \cdot kg^{-1} \cdot K^{-1}}$
C = constant of Eq. 14, $C = 0.9026$
d = internal tube diameter, m
f = Fanning friction factor of NF flow obtained from Eq. 6, 1
f_{LDV} = friction factor NF flow obtained from Eq. 7, where $t_0 = (t_0)_{\mathrm{LDV}}$, 1
f_{dr} = drag-reduction factor $f_{dr} = (f_p/f)_{Re}$, 1
f_{hr} = heat-transfer reduction factor $f_{hr} = (\alpha_p/\alpha)_{Re}$, 1
f_p = Fanning friction factor of a PS flow obtained from Eq. 8, 1
$(f_p)_{\mathrm{LDV}}$ = friction factor PS flow obtained from Eq. 9, where $t_{0,p} = (t_{0,p})_{\mathrm{LDV}}$, 1
k = threshold level in Eq. 16, 1
L = length of pipe section for pressure-drop measurements, m
N, N_p = number of time intervals measured between $(t - \Delta t/2)$ and $(t + \Delta t/2)$, 1
N_0 = total number of time intervals measured in a water flow, 1
$N_{0,p}$ = total number of time intervals measured in a drag-reducer solution flow, 1
R = radius of tube, m
t = time; age of a fluid element at the wall in an NF flow, s
t_d = time at which a renewal is detected (Figure 8), s
t_0 = mean age of fluid elements at the wall in an NF flow, s
$(t_0)_{\mathrm{LDV}} = t_0$ derived from LDV signals, s
$(t_{0,p})_{\mathrm{LDV}} = t_{0,p}$ derived from LDV signals, s
$t_{0,p}$ = mean age of fluid elements at the wall in a PS flow, s
t_p = age of a fluid element at the wall in a PS flow, s
t_s = mean swap time in a NF flow (Eq. 40), s
$t_{s,p}$ = mean swap time in a PS flow (Eq. 40), s
t_r = reference time Eq. 41, s
T = temperature, K
$u(y,t)$ = instantaneous local axial velocity, $\mathrm{m \cdot s^{-1}}$
$\bar{u}(y)$ = time-averaged local axial (TALA) velocity, $\mathrm{m \cdot s^{-1}}$
u' = local axial velocity fluctuation $u(y,t) - \bar{u}(y)$, $\mathrm{m \cdot s^{-1}}$
u_b = average axial fluid velocity in the bulk, $\mathrm{m \cdot s^{-1}}$
$\langle \bar{u} \rangle$ = superficial fluid velocity, $\mathrm{m \cdot s^{-1}}$
$\hat{u}$ = conditionally averaged local axial (CALA) velocity, $\mathrm{m \cdot s^{-1}}$
y = distance from the wall in an NF flow (Eq. 33), m
y_p = distance from the wall in a PS flow (Eq. 33), m
y^+ = dimensionless distance from the wall in an NF flow (Eq. 32), m
y_p^+ = dimensionless distance from the wall in a PS flow (Eq. 32), m
y_{36} = value of y at $y^+ = 36$; Eq. 33a, m
$y_{p,36}$ = value of y_p at $y^+ = 36$; Eq. 33a, m
z = dimensionless variable $z = y(4\nu t)^{-0.5}$, 1
z_0 = dimensionless parameter $z_0 = y(4\nu t_0)^{-0.5}$, 1

Greek letters

α = heat-transfer coefficient in a solvent flow, $\mathrm{W \cdot m^{-2} \cdot K^{-1}}$
α_p = heat-transfer coefficient in a drag-reducer solution flow, $\mathrm{W \cdot m^{-2} \cdot K^{-1}}$
γ = dimensionless quantity defined by $a/t_0 \equiv \gamma = a_p/t_{0,p}$, 1
δ = momentum-transfer thickness of a fluid element with age t in an NF flow, m
$\bar{\delta}$ = time-averaged momentum-transfer thickness in an NF flow, m
δ_p = momentum-transfer thickness of a fluid element with age t_p in a PS flow, m
$\bar{\delta}_p$ = time-averaged momentum-transfer thickness in a PS flow, m
ϵ = dimensionless eye-to-wall distance in NF flow (Eq. 36), 1
ϵ_p = dimensionless eye-to-wall distance in PS flow (Eq. 36), 1
Δ = period defined in Eq. 41, s
Δ_0 = period defined in Eq. 41, s
Δ_p = period defined in Eq. 42, s
Δp = frictional axial pressure drop in NF flow, Pa
Δp_p = frictional axial pressure drop in PS flow, Pa
Δt = small part of age t, s
η = dynamic viscosity of solvent, Pa·s
λ = ratio $\lambda \equiv \delta/\bar{\delta}$ defined in Eq. A9, 1
λ_p = ratio $\lambda_p \equiv \delta_p/\bar{\delta}_p$ defined in Eq. A9, 1
λ_c = thermal conductivity of solvent, $\mathrm{W \cdot m^{-1} \cdot K^{-1}}$
ν = kinematic viscosity of solvent, $\mathrm{m^2 \cdot s^{-1}}$
ρ = density of solvent, $\mathrm{kg \cdot m^{-3}}$
τ_w = instantaneous, local, axial wall-shear stress in an NF flow, Pa
$\tau_{w,p}$ = instantaneous, local, axial wall-shear stress in a PS flow, Pa
$\bar{\tau}_w$ = time-averaged axial wall-shear stress in an NF flow, Pa
$\bar{\tau}_{w,p}$ = time-averaged axial wall-shear stress in a PS flow, Pa
Ψ = density function of δ (Eq. A11), 1
Ψ_p = density function of δ_p (Eq. A11), 1
Ψ_5 = density function defined in Eq. A10, 1

Dimensionless numbers

Re = Reynolds number of solvent flow ($Re \equiv \langle \bar{u} \rangle d/\nu$), 1
Fa = Fanning number of solvent flow $Fa \equiv Re\, f/2$
Fo = Fourier number solvent flow $Fo \equiv \nu t_0/d^2$, 1
Fo_p = Fourier number PS flow $Fo_p \equiv \nu t_{0,p}/d^2$, 1
Nu = Nusselt number solvent flow $Nu \equiv \alpha d/\lambda_c$, 1
Nu_p = Nusselt number PS flow $Nu_p \equiv \alpha_p d/\lambda_c$, 1
Pr = Prandtl number $Pr \equiv C_p \eta/\lambda_c$, 1

Abbreviations

BK = Blackwelder and Kaplan
CALA = conditionally averaged local axial
LDV = laser-Doppler velocimeter
NF = Newtonian fluid/solvent
PS = polymer solution (aqueous solution of 20 mg/kg Separan AP-30)
RSR = random surface renewal
SNR = signal-to-noise ratio
TALA = time-averaged local axial

Literature Cited

Blackwelder, R. F., and R. E. Kaplan, "On the Wall Structure of the Turbulent Boundary Layer," *J. Fluid Mech.*, **76**, 89 (1976).

Danckwerts, P. V., "Significance of Liquid-Film Coefficients in Gas Absorption," *Ind. Eng. Chem.*, **43**, 1460 (1951).

Eck, B., *Technische Strömungslehre*, Vol. 1, Springer-Verlag, New York, p. 95 (1978).

Fortuin, J. M. H., and P.-J. Klijn, "Drag Reduction and Random Surface Renewal in Turbulent Pipe Flow," *Chem. Eng. Sci.*, **37**, 611 (1982).

Fortuin, J. M. H., E. E. Musschenga, and P. J. Hamersma, "Transfer Processes in Turbulent Pipe Flow Described by the ERSR Model," *AIChE J.*, **38**, 343 (1992).

Hamersma, P. J., J. Ellenberger, and J. M. H. Fortuin, "Derivation of a Three-Parameter Model Describing the Results of Steady-State Shear Stress–Shear Rate Measurements of Viscoelastic Polymer Solutions, with Different Types of Equipment in a Seven-Decade Shear-Rate Range," *Chem. Eng. Sci.*, **38**, 819 (1983).

Musschenga, E. E., P. J. Hamersma, and J. M. H. Fortuin, "Momentum, Heat and Mass Transfer in Turbulent Pipe Flow: The Extended Random Surface Renewal Model," *Chem. Eng. Sci.*, **47**, 4373 (1992).

Van Maanen, H. R. E., and J. M. H. Fortuin, "Experimental Determination of the Random Lump-age Distribution in the Boundary Layer of a Turbulent Pipe Flow Using Laser-Doppler Anemometry, *Chem. Eng. Sci.*, **38**, 399 (1983).

Appendix: Model of a Surface Renewal

Experimental CALA velocities

Each point of the CALA velocity profiles presented in Figure 8 has been obtained from a large number of velocities measured at a fixed distance, $t - t_d$, from the detection time, t_d, using LDV. An average velocity profile of a surface renewal can be expected when an old fluid element at the wall has a mean age t_0 for an NF flow or $t_{0,p}$ for a PS flow. The TALA velocities can be obtained from Eqs. 36 to 38

- NF flow $(y = y_{36})$ — $\bar{u}(y_{36}) = \langle\bar{u}\rangle\{1 - \exp(-\epsilon)\}$
- PS flow $(y_p = y_{p,36})$ — $\bar{u}_p(y_{p,36}) = \langle\bar{u}\rangle\{1 - \exp(-\epsilon_p)\}$ (A1)

$$\epsilon = \frac{y_{36}}{\sqrt{\nu t_0}} = \frac{36}{\sqrt{2/f}} = \frac{7.08}{\log(Re/7)}$$

$$\epsilon_p = \frac{y_{p,36}}{\sqrt{\nu t_{o,p}}} = \frac{36\sqrt{f_{dr}}}{\sqrt{2/F}} = \frac{7.08\sqrt{f_{dr}}}{\log(Re/7)}. \quad \text{(A2)}$$

At a surface renewal, an inrushing fluid element from the bulk with an axial velocity $u_b \approx \langle\bar{u}\rangle$ in an NF flow and $u_{b,p} \approx \langle\bar{u}\rangle$ in a PS flow is assumed to penetrate between the old one and the wall, while the old one is swapped into the bulk. During this renewal, the velocity profile in the old fluid element and that in the new one, which successively pass the eye in the direction of the bulk, are recorded by LDV. Figure 8 shows that the CALA velocity profile during each renewal consists of three regions bounded by a minimum and a maximum CALA velocity

- NF flow $(y = y_{36})$ — $\bar{u}(y_{36}) > \hat{u} > \hat{u}_{\min}$ — PS flow $(y_p = y_{p,36})$ — $\bar{u}(y_{p,36}) > \hat{u}_p > \hat{u}_{p,\min}$ Region 1 (A3)

$\hat{u}_{\min} < \hat{u} < \hat{u}_{\max}$ — $\hat{u}_{p,\min} < \hat{u}_p < \hat{u}_{p,\max}$ Region 2 (A4)

$\hat{u}_{\max} > \hat{u} > \bar{u}(y_{36})$ — $\hat{u}_{p,\max} > \hat{u}_p > \bar{u}(y_{p,36})$ Region 3 (A5)

The CALA velocity decreases from the TALA velocity to a minimum CALA velocity $\hat{u}_{\min} \approx \langle\bar{u}\rangle/2$; this minimum can be considered as the velocity of the interface where the new fluid element with an original axial velocity $u_b \approx \langle\bar{u}\rangle$ contacts the old one with an original axial velocity zero at the wall. The maximum axial velocity $\hat{u}_{\max}$ approaches the superficial velocity $\langle\bar{u}\rangle$. Then, the CALA velocity decreases and approaches the TALA velocity again.

Simulated CALA velocities

The instantaneous velocity profile of each laminar coherent fluid structure at the wall is dependent on its age and can be obtained from Eq. 2

$$u(y,t) = u_b \,\mathrm{erf}(z), \qquad \text{where} \qquad z = y/\sqrt{4\nu t}. \quad \text{(A6)}$$

The instantaneous momentum-transfer thickness, δ, of such a single coherent fluid structure is the thickness of a laminar layer of constant velocity gradient that transfers equal momentum to the wall as the fluid element with the velocity profile of Eq. A6. Consequently, the instantaneous momentum-transfer thickness, δ, of this fluid element follows from Eq. A6

$$\nu\rho u_b/\delta = \tau_w = \eta(du/dy)_{y=0} = \nu\rho u_b/\sqrt{\pi\nu t}; \qquad \delta = \sqrt{\pi\nu t}. \quad \text{(A7)}$$

The time-averaged momentum-transfer thickness is obtained from Eq. 5

$$\nu\rho u_b/\bar{\delta} = \bar{\tau}_w = \eta(d\bar{u}/dy)_{y=0} = \nu\rho u_b/\sqrt{\nu t_0}; \qquad \bar{\delta} = \sqrt{\nu t_0} = d/Fa. \quad \text{(A8)}$$

Equations A7 and A8 yield the relative instantaneous momentum-transfer thickness

$$\lambda \equiv \delta/\bar{\delta} = \sqrt{\pi t/t_0}; \quad t/t_0 = \left(\lambda/\sqrt{\pi}\right)^2; \qquad d(t/t_0) = \left(\lambda\sqrt{2/\pi}\right)d\left(\lambda\sqrt{2/\pi}\right). \quad \text{(A9)}$$

The ratio λ_p is obtained in a similar way. If Ψ_5 (Fortuin and Klijn, 1982) represents the density function of the relative momentum-transfer thickness, the following relationship holds

$$\Psi_5 d\lambda = \exp(-t/t_0)d(t/t_0). \quad \text{(A10)}$$

Combining Eqs. A9 and A10 leads to the following relative instantaneous momentum-transfer thickness distribution of coherent fluid structures at the wall

$$\Psi_5 d\lambda = \Psi d\left(\lambda\sqrt{2/\pi}\right) = \left(\lambda\sqrt{2/\pi}\right)\left(\exp\left(-0.5\left(\lambda\sqrt{2/\pi}\right)^2\right)d\left(\lambda\sqrt{2/\pi}\right)\right). \quad \text{(A11)}$$

Assuming that at given values of $\langle\bar{u}\rangle$, d, and ν the wall-to-bulk velocity, u_{wb}, of the interface between a new and an old fluid element is constant and equal for each surface renewal, the time Δ needed for a shift δ of this interface in the wall-to-bulk direction follows from

$$\Delta = \delta/u_{wb} \quad \text{(NF flow)}; \qquad \Delta_p = \delta_p/u_{wb,p} \quad \text{(PS flow)}. \quad \text{(A12)}$$

Defining the empirical constants

$$\Delta_0 \equiv \sqrt{\pi/2}\,\bar{\delta}/u_{wb} \quad \text{(NF flow)}; \qquad \Delta_{0,p} \equiv \sqrt{\pi/2}\,\bar{\delta}_p/u_{wb,p} \quad \text{(PS flow)}, \quad \text{(A13)}$$

Eqs. A9, A12, and A13 result in

$$\lambda\sqrt{2/\pi} = \Delta/\Delta_0; \qquad \lambda_p\sqrt{2/\pi} = \Delta_p/\Delta_{0,p}; \qquad u_{wb} = \sqrt{\pi/2}\,\bar{\delta}/\Delta_0; \qquad u_{wb,p} = \sqrt{\pi/2}\,\bar{\delta}_p/\Delta_{0,p}. \quad \text{(A14)}$$

As a consequence, Eqs. A11 and A14 lead to

$$\Psi = (\Delta/\Delta_0)\exp\left(-0.5\Delta^2/\Delta_0^2\right); \qquad \Psi_p = \left(\Delta_p/\Delta_{0,p}\right)\exp\left(-0.5\Delta_p^2/\Delta_{0,p}^2\right). \quad \text{(A15)}$$

The TALA velocities at $y = y_{36}$ and $y_p = y_{p,36}$ follow from Eqs. 36 and 38

$$\hat{u}(y_{36}) = \langle\bar{u}\rangle\{1-\exp(-\epsilon)\}, \qquad \text{where} \quad \epsilon = y_{36}/\sqrt{\nu t_0}$$

and

$$\hat{u}_p(y_{p,36}) = \langle\bar{u}\rangle\{1-\exp(-\epsilon_p)\}, \qquad \text{where} \quad \epsilon_p = y_{p,36}/\sqrt{\nu t_{0,p}}. \quad \text{(A16)}$$

The CALA velocities follow from

$$\hat{u}(y_{36}) = \langle\bar{u}\rangle[1-\exp\{-\epsilon(1+\Psi)\}]; \qquad \hat{u}_p(y_{p,36}) = \langle\bar{u}\rangle\left[1-\exp\left\{-\epsilon_p\left(1+\Psi_p\right)\right\}\right]. \quad (17)$$

Equations A15 and A17 yield the following CALA velocities

$$\hat{u}(y_{36}) = \langle\bar{u}\rangle\left[1-\exp\left\{-\epsilon\left[1+(\Delta/\Delta_0)\exp\left(-0.5\Delta^2/\Delta_0^2\right)\right]\right\}\right] \quad \text{at} \quad y^+ = 36$$

and

$$\hat{u}_p(y_{p,36}) = \langle\bar{u}\rangle\left[1-\exp\left\{-\epsilon_p\left[1+\left(\Delta_p/\Delta_{0,p}\right)\exp\left(-0.5\Delta_p^2/\Delta_{0,p}^2\right)\right]\right\}\right] \quad \text{at} \quad y_p^+ = 36. \quad \text{(A18)}$$

The extreme CALA velocities are obtained, when

$$\partial\hat{u}(y_{36})/\partial(\Delta/\Delta_0) = 0; \qquad \partial\hat{u}(y_{p,36})/\partial\left(\Delta_p/\Delta_{0,p}\right) = 0. \quad \text{(A19)}$$

The equations for calculating CALA velocities and the minimum and maximum values are presented in Table 4. In Table 3, the values on the lines with the reference Figure 8 were derived from LDV signals and plotted in Figure 8. These values yield the swap times t_s and $t_{s,p}$ (Eq. 40) and the reference time t_r (Eq. 41). The values $\Delta_{\min}$, $\Delta_{\max}$, $\Delta_{p,\min}$, and $\Delta_{p,\max}$ in Table 3 were obtained with Eq. 42.

The time-averaged momentum-transfer thicknesses $\bar{\delta}$ and $\bar{\delta}_p$, also presented in Table 3, were derived from Eqs. 25 and 26 and $R = 25.5$ mm. The velocities u_{wb} and $u_{wb,p}$ of Table 3, derived from Eqs. A14, show that each wall-to-bulk velocity is a fraction of the superficial velocity, increases with increasing Reynolds numbers, and decreases if a drag reducer is added. Table 3 shows that t_s/t_0 and $t_{s,p}/t_{0,p}$ have small constant values $(24 \pm 2)\times 10^{-3}$ at different Reynolds numbers with and without a drag reducer. This justifies the assumption that t_s is approximately proportional to t_0, which was made in the subsection titled "Detection Parameters a and k." The shift $t_d - t_r$ is presented in the last line of Table 3.

Discussion

The equations for simulating the CALA velocities contain the parameters $\langle\bar{u}\rangle$, $\epsilon = y/\sqrt{\nu t_0}$, and Δ_0. The error in $\langle\bar{u}\rangle$ is about 0.2%, as was elucidated in the subsection "Pipe and Fluids." The errors in the calculated parameter, ϵ, and the empirical parameter, Δ_0, are larger and partly due to the following approximations and assumptions:

- The distance y between eye and wall can only be defined and adjusted with a restricted accuracy. More particularly, at a high Reynolds number ($Re = 43{,}400$) of a water flow, where the ratio of the length of the eye ($b = 214$ μm) and the eye-to-wall distance ($y = 816$ μm) is relatively large.
- The assumption that the wall is flat, so that Eq. 1 can be applied, and that the bulk velocity is equal to the superficial velocity ($u_b \approx \langle\bar{u}\rangle$), so that in the equations of Table 4 $\langle\bar{u}\rangle$ can be used instead of u_b.
- The use of the empirical correlation Eq. 19 for all turbulent fluid flows in the glass tube to calculate t_0.

• The assumption that at a surface renewal in a turbulent pipe flow the wall-to-bulk velocity of the interface between an old and a new fluid element is constant at given values of $\langle \bar{u} \rangle$, ν, and d, so that Eqs. A12 and A13 can be applied.

• The difference between t_0, derived from pressure gradients (Eq. 19), and $(t_0)_{\mathrm{LDV}}$ obtained from LDV signals (Figure 3) also indicates the possible error in t_0.

• The assumption that the velocity profiles in the old fluid element and those in the new one pass the eye so rapidly in the wall-to-bulk direction that no correction for momentum diffusivity in these fluid elements is needed.

• The local apparent viscosity of the PS flow at the tube wall is assumed to be independent of the local shear stress and to be equal to the solvent viscosity. The drag-reduction factor is assumed to be independent of the temperature.

Summarizing, it can be stated that in spite of approximations and assumptions, the agreement between measured and simulated values of both TALA and CALA velocities justifies the conclusion that the model derived in this appendix contributes to a better understanding of the mechanism of single surface renewals in turbulent fluid flows with and without a drag reducer.

Manuscript received Oct. 3, 2001, and revision received July 18, 2002.